Transient local entropy generation analysis for the design improvement of a thermocline thermal energy storage

Transient Local Entropy Generation Analysis for the Design Improvement of a Thermocline Thermal Energy Storage

Pizzolato[a], A: Sciacovelli[b], V. Verda[a],

[a] Department of Energy, Politecnico di Torino, Corso Duca degli Abbruzzi 24, 10129, Torino, Italy, alberto.pizzolato@polito.it, vittorio.verda@polito.it

[b] School of Chemical Engineering., Birmingham Centre for Energy Storage (BCES), University Of Birmingham, UK, a.sciacovelli@bham.ac.uk

Abstract

Second-law methodologies for the design improvement of Thermal Energy Storage (TES) systems are complicated by the fact that TES charging and discharging are highly dynamic (i.e. unsteady) in nature and most of the works done in the field consist of black-box parametric studies, where no information at the local level can be obtained by the analyst.

In the present paper, we aim at filling this gap by the introduction of three novel indicators, namely the cumulated local exergy destruction, the characteristic time and the lifespan of entropy generation. These figures of merit provide the designer with a powerful tool that facilitates the identification of the temporal and spatial location of criticalities and the development of design improvements. To test the effectiveness of this innovative methodology, we focused on the design improvement of a molten salts thermocline TES tank for Concentrated Solar Power applications.

We found that analyzing the cumulated exergy destruction only is a blind way to proceed because very limited insights can be obtained on the physical phenomenon. In this case, the total irreversibilities can be reduced only of a 7 % and a 12 % with the help of a porous and a solid baffle respectively. On the other hand, the simultaneous examination of the three parameters allows to generate a far better design by the use of a compounded baffle, able to reduce the total entropy generation of more than 60% compared to the initial configuration.

Highlights

- A methodology for local entropy generation analysis of unsteady processes is needed
- We propose three indicators to locate irreversibilities in both space and time
- We apply these novel tools for the design improvement of a thermocline TES
- The total entropy generation during the discharging is reduced by more than 60 %

Keywords: Local Entropy Generation Analysis; Thermal Energy Storage; Transient processes;

Nomenclature

Latin and Greek letters

Symbol	Quantity	SI Unit
Be	Bejan number	

E	Total Energy	J/m^3
F	Volumetric force	N/m^3
k	Thermal conductivity	W/m K
P	Pressure	Pa
Pr	Prandtl number	
s	Specific entropy	J/K m^3
t	Time	s
T	Temperature	K
u	Velocity	m/s
μ	Dynamic viscosity	Pa s
ρ	Density	Kg/m^3
σ	Viscous stresses	Pa
e	Specific exergy	J/m^3

Subscripts

T	Turbulent
gen	Generated
h	Heat flux related
μ	Viscous stresses related
p	Produced

1. Introduction

Entropy generation driven design methodologies for the performance improvement of engineering systems have met broad acceptance among the scientific community. However, their application to the analysis of strongly unsteady processes, such as TES charging and discharging, is quite complicated: the optimization of the design involves the search for an optimal time history, i.e. the one that minimizes the global entropy produced during a finite time interval. As a consequence, according to [1], very few researchers dedicated to the study of the thermodynamic performances of a TES system under unsteady conditions. The majority of them adopted a lumped parameter (i.e. 0D or black-box) approach, where no or little information is gathered on local phenomena. For instance, in one of the earliest study of this type, Bejan [2] developed a simplified black box model considering the heat capacity of the storage element and the global heat transfer coefficient between Heat Transfer Fluid and storage medium, demonstrating the existence, from a second-law perspective, of an optimal charging and discharging time.

The application of second-law analysis to thermal storage has been particularly focused on Phase Change Material as discussed in the recent review of Jegadheeswaran et al. [3]. In this field, a good number of studies were performed where more detailed black-box models have been implemented [4-6]. As far as high temperature molten salts storage is concerned, Yang et al. [7] proposed to use the global entropy generation as a useful criterion for the selection of a suitable filler material. A more refined model to investigate how the granule diameter of the filler in a thermocline molten salts TES influences the heat transfer and the thermodynamic efficiency was made by Flueckiger and Garimella [8]. However, despite having adopted a CFD model for the solution of the thermo-fluid dynamics problem, their second-law analysis was performed only at the global level and local information was not exploited to propose improved designs.

It should be noted at this point that a wise post-processing of the results of CFD simulations allows to calculate the local distribution of entropy generation, providing the designer with the so-called entropy generation maps. This approach has been often coupled to a heuristic pseudo-optimization methodology [9-12] in which the analyst identifies the most critical regions of the device and proposes effective improvements.

To the knowledge of the Authors, the unique application of the local approach for the design improvement of a transient process is the work of Guelpa et al. [13], who proposed a modification of the fin arrangement in a latent heat TES suggested by the analysis of local entropy generation at different instants of time. The final

configuration was selected as the one enhancing heat transfer and boosting the second law performances of the device during the whole duration of the process.
Despite this last example, we feel that there is a considerable gap in the literature addressing the thermodynamic optimization of transient processes and systems. Hence, the aim of this paper is to provide the analyst/designer with innovative tools for the study of this type of phenomena and to help to clarify not only the spatial but also the temporal location of irreversibilities.
In order to show the effectiveness of the methodology proposed, we focused on the design improvement of the 1.3 MWh_t thermocline (i.e. single-tank) TES system located at the ENEA research centre La Casaccia (Rome). In the first part of the paper, we present the 2D CFD model, accounting for fluid-flow and heat transfer, which we used for the investigation of the thermo-fluid dynamic behaviour of the tank. Then, the CFD model, is used to perform a first Entropy Generation Analysis (EGA) where two possible improvements are identified. Finally, with the help of two innovative figures of merit that keeps into account the temporal evolution of the process, a final design is proposed and evaluated.

2 .System description and numerical model

The thermocline TES system at the research centre La Casaccia consists of a single tank with diameter D = 2 m and height H= 2.2 m. The storage medium is molten salt (60% NaNO3 and 40% KNO3 on mass basis) with operating temperatures ranging from 280 °C to 550 °C and the steam generator is fully integrated in the TES, as detailed in [15]. A bi-dimensional axial-symmetric representation of the system is given in the left side of Figure 1. The internal cavity represents the external envelope of the integrated steam generator, whose radius measures 0.125 m. From a careful examination of its shape, it is possible to notice a Venturi tube at the bottom, which has the aim of slowing down the fluid during the discharge of the tank and avoid mixing due to inlet effects.
Due to the high velocity in the inlet region, we have chosen to adopt a turbulent model in which, assuming negligible fluctuations in density, viscosity and thermal conductivity, the continuity, momentum and energy equations can be written as follows:

$$\frac{\partial \rho}{\partial t} + \frac{\partial \rho u_j}{\partial x_j} = 0 \tag{1}$$

$$\frac{\partial \rho u_i}{\partial t} + \frac{\partial \left(\rho u_i u_j\right)}{\partial x_j} = -\frac{\partial P}{\partial x_i} + \frac{\partial \sigma_{ij}}{\partial x_j} + F_i \tag{2}$$

$$\frac{\partial \rho E}{\partial t} + \frac{\partial \left(\rho u_j H\right)}{\partial x_j} = \frac{\partial \left(u_i \sigma_{ij}\right)}{\partial x_j} - \frac{\partial}{\partial x_j}\left(\left(\frac{\mu}{\mathrm{Pr}} + \frac{\mu_T}{\mathrm{Pr}_T}\right)\left(\frac{\partial T}{\partial x_j}\right)\right) \tag{3}$$

where:

- σ_{ij} is the tensor of viscous stresses defined as:

$$\sigma_{ij} = 2\left(\mu + \mu_T\right)\left(S_{ij} - \frac{1}{3} S_{kk}\delta_{ij}\right) \tag{4}$$

- S_{ij} is the tensor of shear stresses defined as:

$$S_{ij} = \frac{1}{2}\left(\frac{\partial u_i}{\partial x_j} + \frac{\partial u_j}{\partial x_i}\right) \tag{5}$$

- H is the total enthalpy:

$$H = E + \frac{P}{\rho} \tag{6}$$

For the closure of the equation set, the two-equation $k-\omega$ model has been implemented, which consists of solving for two additional variables: k, the turbulent kinetic energy, and ω, the specific rate of dissipation of kinetic energy.

The governing equations are converted to algebraic equations using the finite-element technique in COMSOL. The discretization strategy adopted utilizes 2nd order Lagrange finite elements to model the velocity components and linear elements to model the pressure field. The time integrations scheme is a fully-implicit variable-order variable-time step BDF (Backward Differentiation Formula).

As far as the computational grid is concerned, we have chosen a free-triangular mesh with about 40k elements slightly stretched in the radial direction in order to obtain characteristic dimensions of 1.5 cm and 0.5 cm along the radial and axial direction respectively. This choice is the result of a previous grid-convergence study.

In order to test the validity of the model we have simulated a complete discharging process and we have compared the results to the experimental data gathered at La Casaccia Research Centre with the experimental instrumentation described in Ref. [14]. The comparison of the simulated temperature profile versus the experimental data obtained during the discharging of the ENEA tank is shown in the right side of Figure 1. The mean absolute error is calculated to be 1.18 K with a standard deviation of 2.53 K. This close agreement indicates that the numerical model is able to reproduce the tank discharging process accurately and it can be confidently used for the following entropy generation analysis.

3 Entropy generation analysis and pseudo-optimization

TES charging and discharging processes are highly dynamic (i.e. unsteady) in nature, therefore traditional steady-state second law analysis cannot be used. In this work, we have maintained the local approach but, instead of the rate of local exergy destruction, we have a considered the cumulated exergy destroyed defined as:

$$e_d(\mathrm{r},t) = T_0 \int_0^t s_{gen}(\mathrm{r},t)dt \tag{6}$$

Where the reference temperature T_0 has been set to 298.15 K.

In thermo-fluid dynamics problems, two main factors are responsible of thermodynamic irreversibilities, namely heat transfer and viscous dissipation. Hence, the local specific entropy production per unit volume s_p can be written as:

$$s_p = s_h + s_\mu \tag{7}$$

where:

- s_h is the contribution of heat transfer to the local entropy generation
- s_μ is the contribution of fluid friction to the local entropy generation

If local equilibrium is assumed, it is possible to write [1]:

$$s_h = \frac{\mathbf{J}_q \cdot \nabla T}{T^2} \tag{8}$$

$$s_\mu = \frac{1}{T}\sigma : \nabla \mathbf{v} \tag{9}$$

Where:

- $\mathbf{J_q}$ is the heat flux, computed as
$$\mathbf{J}_q = -(k + k_T) \cdot \nabla T \quad (10)$$
- $\nabla \mathbf{v}$ is the gradient of the velocity vector
- $\boldsymbol{\sigma}$ is the stress tensor computed as in Eq. (4)

In order to quantify the relative importance of these two factors, we used the Bejan number Be, which is defined as:

$$Be = \frac{s_h}{s_\mu + s_h} \quad (11)$$

that is the ratio of heat transfer irrevesibilities to the total irreversibilities. In the discharging process previously described, we have calculated the local Bejan number to be always higher 0.99. This means that heat transfer irreversibilities are at least two order of magnitude greater than viscous ones and that this last contribution can be neglected without compromising the results of the analysis.
The discharging process that we have validated in the previous section, has been investigated using the tools described above. Referring to Figure 2, the analysis of the entropy generation map, shows that a very localized region close to the inlet, is responsible of an local exergy destruction of one order of magnitude larger than any other region of the tank. Moving to less irreversible regions, the region with a local exergy destruction in the order of 10^8 J/m^3 corresponds to the area interested by the thermocline transit. On the other hand, the region that features a cumulated local exergy destruction in the order of 10^7 J/m^3 has not been reached by the thermocline by the end of the process. Surprisingly enough, buoyancy induced currents due to thermal losses at the tank wall are responsible of a small fraction of irreversibilities, exception made for the bottom curvy wall. It is clear that a closer look should be taken at the physics of the process to understand the reasons of such a high irreversibilities concentration near the inlet. From the analysis of the temperature map and the streamlines displayed on the right side of Figure 2, it has been noticed that the high density of cumulated exergy destroyed near the inlet is due to the presence of a strong recirculating current, which brings together fluid particles at a very different temperature creating large temperature gradients and strong irreversible thermal fluxes. Hence, two alternatives were proposed to conveniently modify the flow field and limit the magnitude of the mixing eddies shown in the right side of Figure 2:

- A 3 cm thick porous baffle, linking the border of the inlet section to the tank bottom surface with an inclination of 30 ° with respect to the vertical. The longitudinal and radial permeabilities have been set to $3\,x\,10^{-8}\ m^2$ and $1\,x\,10^{-9}\ m^2$ respectively in analogy to [16]. In this first modification the flow area is maintained equal to the original design.
- A 3 cm thick solid baffle, placed exactly in the same position as the porous one but leaving a 2 cm channel to allow the fluid flow at the bottom of the tank- This second modification brings a slight flow area reduction of 0.18% making the two modifications still comparable.

The exergy destruction fields of the discharging process for the two design of the tank with porous baffle and solid baffle are shown in Figure 3, where also five streamlines at $t = 1000\ s$ are represented to illustrate the flow path. The porous barrier, although limiting the recirculating flow, boosts the exergy destruction on the baffle side facing the upper region of the tank. In fact, since the cold fluid crosses the permeable layer following the normal direction, it reaches a higher elevation than the one that could be calculated with an ideal stratification model, in which the axial position of a fluid particle can be determined according to hydrostatic equilibrium once its temperature, and thus its density, is known. As a result, the colder stream encounters hotter fluid creating a buoyancy-driven eddy. On the other hand, the solid baffle looks a better choice: a very small mixing eddy is confined in the baffle-delimited region thus reducing the area affected by thermodynamic irreversibilities. The global exergy destruction rate, calculated as the integral over the tank volume V of the local exergy destruction rate, is presented in Fig. 4 (left side) for the three designs of the tank considered. Similarly,

Fig. 4 right depicts the cumulated global exergy destruction obtained by integrating over the volume V the cumulated exergy destruction defined by Eq. (6). Consequently, the exergy destroyed over the entire discharging process of the tank coincides with the value of the cumulated exergy destruction at the last instant of time considered, i.e. t = 4400 s (Fig. 4 right). Fig. 4 right indicates that the porous and the solid baffle bring respectively a 7 % and a 12 % reduction of the cumulated exergy destroyed over the entire process. However, from the analysis of the exergy destruction rate (Figure 4, left side), it can be seen that the two designs proposed bring performance improvements at different time intervals of the discharge process. In particular, the utilization of the porous baffle smooths considerably the initial peak of entropy generation with respect to the solid one but it causes a higher entropy generation rate in the second part of the process (t > 2000s). An interesting consequence of this observation is that, if the process is stopped at t=2000 s, the best design modification would have been the porous baffle, showing that a deeper understanding should be obtained on the dynamic nature of the process. In the next section, additional tools for the local EGA of transient processes will be introduced, allowing the analyst/designer to further improve the design optimization strategy.

4 Refined analysis

The heuristic approach adopted in the previous section has brought us to improved designs of the tank presenting two kind of baffles near the inlet section. However, such approach based on the analysis of the maps of cumulated exergy destruction (Eq. 6) and the corresponding global exergy destruction rate (Fig. 4) do not provide conclusive details about the *temporal distribution* and *temporal extent* of the thermodynamic irreversibility for a transient process, such as the discharge of the storage tank here investigated. To overcome these drawbacks we propose two novel indicators that stem from statistical analysis. The first one is the characteristic time of entropy generation $\bar{t}$ defined as:

$$\bar{t}(\mathbf{r}) = \frac{\int_0^{t_{end}} s_p(\mathbf{r},t)\cdot t dt}{\int_0^{t_{end}} s_p(\mathbf{r},t) dt} \tag{12}$$

If, in analogy, the local entropy generation at a particular position $\boldsymbol{r}$ is considered as a statistical distribution, the characteristic time of entropy generation indicates *when* on average entropy is generate at such particular location **r**. However, such indicator does not provide any detail about the time extent of entropy generation at position **r.** To this aim, we propose to adopt a second indicator named *entropy generation lifespan*:

$$\sigma_t = \sqrt{\frac{\int_0^{t_{end}} s_p(\mathbf{r},t)\cdot t^2 dt}{\int_0^{t_{end}} s_p(\mathbf{r},t) dt} - \bar{t}^2} \tag{13}$$

From the previous definition it can be noticed that σ_t formally coincides with the standard deviation of the entropy generation rate s_p. In fact, σ_t quantifies the *extent of the period,* in which entropy is generated at position **r** of the computational domain that is the lifespan of the entropy generation.
The simultaneous analysis of the three figures of merit clarifies *where* the most critical regions are located, *when* irreversibilities are generated and for *how long*. In order to propose effective design modifications, the analyst can now focus his investigations efforts on a limited region and in a *limited period of time*. The design improvement procedure is thus modified as follows:

1. Formulation of initial design and mathematical model
2. Solution of the governing equations through a numerical model
3. Calculation of cumulated exergy destroyed e_d, entropy generation characteristic time $\bar{t}$ and entropy generation lifespan σ_t
4. Investigation of the reasons behind the criticalities, focusing the effort on the most critical region and on the most critical period of time
5. Proposal of design modifications
6. Test of the performances of the new design

For the process considered in the framework of the present work, we performed the third step on the list for the design with the solid baffle and with the porous baffle. The 2D maps obtained are given in Figure 5 and in Figure 6 respectively. Similar trends and crucial differences emerge from the comparative analysis of the two additional parameters for the design cases considered. Starting from the formers, we can divide the storage tank in three regions with distinctive features. The first one is the region delimited by the baffle, which shows a very high concentration of irreversibilities that are generated in the very initial instants of time of the process considered. In fact both the characteristic time and the time standard deviation are very low: ~200 s and ~400 s respectively. The second region, covering the tank axial dimension up to $z = 1\ m$, corresponds to the elevation of the outlet section. In this region, the characteristic time increases with height and the time standard deviation is fairly constant: this portrait corresponds to the thermocline transit that brings into the region intrinsic irreversibilities due thermal diffusion. The last region covers the remaining part of the geometry, with a low value of cumulated irreversibilities that are generated quite constantly during the whole duration of the process with a symmetric distribution around the mean value of 2000 s, which is very close to the median time of the process. In this region, located above the outlet section of the tank, the fluid is nearly still and the only motion is due to weak buoyancy currents induced by thermal losses on the top free layer.
To identify relevant differences among the two cases considered and try to explain the results presented in Figure 4, a detail of the three indicators over the inlet region is illustrated in Fig. 7. In the case of the solid baffle (Figure 7 (a), (b) and (c)), it is possible to conclude that a large fraction of irreversibilities is generated in the inlet region in the initial period of the discharge process where the mixing due to the inlet jet is all constrained into a fixed volume. On the other hand, the higher tip of the porous baffle on the external side is very critical and in that area the characteristic period of exergy destruction is roughly centered around 1000 s with a standard deviation of 800 s. This is the key factor responsible for the trend highlighted in Figure 4, where the porous baffle creates larger irreversibilities than the other options in the intermediate phase of the process (t ~ 2000 ± 1000 s). An intuitive physical explanation is obtainable by looking again at the flow path of Figure 3: it can be noticed that the discontinuity introduced by the porous baffle radically modifies the flow path. In fact, part of the fluid that just entered the domain is driven by the porous baffle right in the middle of the thermocline, enhancing unwanted mixing effect. This behavior lasts until the thermocline zone is all above the higher tip of the baffle.

5 Final design

The transient local EGA presented in the previous section shown that the two modifications proposed have both advantages and drawbacks and that a tradeoff between the two has the potential to ameliorate the overall performances. In particular, the ideal baffle should be able to conveniently modify the flow path in the initial period and to inject cold fluid at the lowest elevation possible during the whole duration of the process. Figure 8 shows a convenient combination of the solid and porous baffle. The blue area is the inlet-delimited region, the porous baffle is highlighted in red, the solid baffle is the white layer protruding into the geometry and the remaining part of the computational domain is in green.
The results obtained for the compound baffle of Fig. 8 are shown in Figure 9. The cumulated exergy destroyed of the final design is considerably reduced compared to the first two improvements proposed. In fact, the modified inlet configuration allows to decrease the total irreversibilities generated to 61 MJ from the initial 156 MJ, i.e. a 60.9 % reduction. Furthermore, it is interesting to observe how great improvements were achieved

with respect to the initial design proposed, whose irreversibilities have been reduced of 54.5 % and 50.4 % for the solid and porous baffle case respectively. As a matter of fact, from the analysis of the trend of exergy destruction rate (Figure 9, left side), it is clear that the compounded baffle outperforms the two other design for nearly all the duration of the process

Conclusions

In the present work, we addressed the need for a reliable methodology allowing to quantify the thermodynamic performances of transient processes both at the local and at the global level. To test our approach, we used a validated CFD model to perform a second-law analysis and a pseudo-optimization of a molten salts TES during a complete discharge process.

In the first part of the work, we showed that the analysis of the cumulated exergy destruction allows one to identify and localize the main sources of irreversibilities. It has been highlighted that the region near the inlet is the most critical one due to a strong recirculating flow and considerable performance improvements can be obtained with limited efforts. In fact, the utilization of a porous layer can reduce the entropy generated in the process considered of 7 %, while the inclusion of a solid baffle has the potential to decrease the total irreversibilities of an additional 5 %.

However, the utilization of cumulated local exergy destruction still hides to the designer a precise temporal characterization of the physical phenomenon. Hence, we propose two novel indicators, i.e. the lifespan and the characteristic time of entropy generation, which provide some key insights to the study of unsteady processes. Using these additional figures of merit, we have been able to design a new baffle (partly solid and partly porous) that reduces the total irreversibilities of more than 60 % and improves the thermodynamic efficiency of the process from 69 % to 87 %.

References

[1] Sciacovelli, A., Verda, V., & Sciubba, E. (2015). Entropy generation analysis as a design tool—A review. Renewable and Sustainable Energy Reviews, 43, 1167-1181.

[2] Bejan, A. (1978). Two thermodynamic optima in the design of sensible heat units for energy storage. Journal of Heat Transfer, 100(4), 708-712.

[3] Jegadheeswaran, S., Pohekar, S. D., & Kousksou, T. (2010). Exergy based performance evaluation of latent heat thermal storage system: a review. Renewable and Sustainable Energy Reviews, 14(9), 2580-2595.

[4] Strub, F., & Bédécarrats, J. P. (1999). Numerical second law analysis of a refrigeration phase-change storage. International Journal of Thermodynamics, 2(3), 133-138.

[5] Kousksou, T., Strub, F., Lasvignottes, J. C., Jamil, A., & Bedecarrats, J. P. (2007). Second law analysis of latent thermal storage for solar system. Solar energy materials and solar cells, 91(14), 1275-1281.

[6] Erek, A., & Dincer, I. (2008). An approach to entropy analysis of a latent heat storage module. International Journal of Thermal Sciences, 47(8), 1077-1085.

[7] Yang, X., Yang, X., Ding, J., Shao, Y., Qin, F. G., & Jiang, R. (2012). Criteria for performance improvement of a molten salt thermocline storage system. Applied Thermal Engineering, 48, 24-31.

[8] Flueckiger, S. M., & Garimella, S. V. (2012). Second-law analysis of molten-salt thermal energy storage in thermoclines. Solar Energy, 86(5), 1621-1631

[9] Iandoli, C. L., & Sciubba, E. (2005). 3-D numerical calculation of the local entropy generation rates in a radial compressor stage. International journal of thermodynamics, 8(2), 83.

[10] Sciacovelli, A., Guelpa, E., & Verda, V. (2014). Second Law Optimization of a PCM Based Latent Heat Thermal Energy Storage System with Tree Shaped Fins. International Journal of Thermodynamics, 17(3).

[11] Sciacovelli, A., & Verda, V. (2009). Entropy generation analysis in a monolithic-type solid oxide fuel cell (SOFC). Energy, 34(7), 850-865.

[12] Sciacovelli, A., & Verda, V. (2011). Entropy generation analysis for the design optimization of solid oxide fuel cells. International Journal of Numerical Methods for Heat & Fluid Flow, 21(5), 535-558.

[13] Guelpa, E., Sciacovelli, A., & Verda, V. (2013). Entropy generation analysis for the design improvement of a latent heat storage system. Energy, 53, 128-138.
[14] Pizzolato, A., Donato, F., Verda, V., & Santarelli, M. (2015). CFD-based reduced model for the simulation of thermocline thermal energy storage systems. Applied Thermal Engineering, 76, 391-399.
[15] Gaggioli, W., Fabrizi, F., Fontana, F., Rinaldi, L., & Tarquini, P. (2014). An innovative concept of a thermal energy storage system based on a single tank configuration using stratifying molten salts as both heat storage medium and heat transfer fluid, and with an integrated steam generator. Energy Procedia, 49, 780-789.
[16] Brown, N. M., & Lai, F. C. (2011). Enhanced thermal stratification in a liquid storage tank with a porous manifold. Solar Energy, 85(7), 1409-1417.

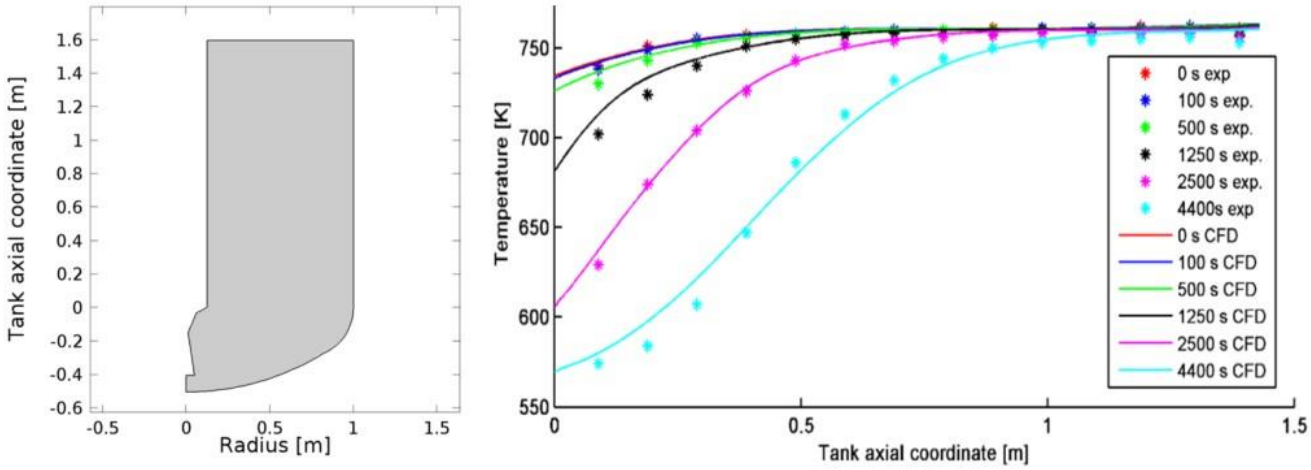

FIGURE 1. Left: geometry considered. Right: Validation of the CFD model with experimental data

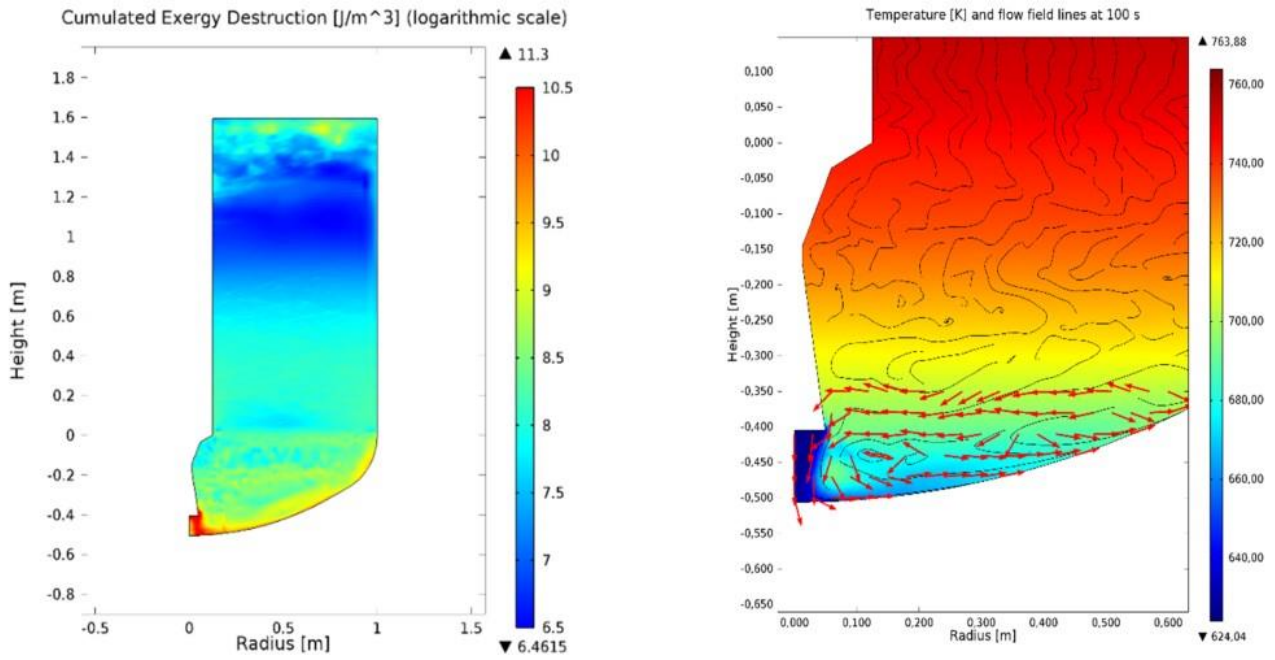

FIGURE 2. Left: Cumulated exergy destroyed distribution (logarithmic scale) at 4400 s. Right: Flow field and temperature distribution in the region close to the inlet at 100 s

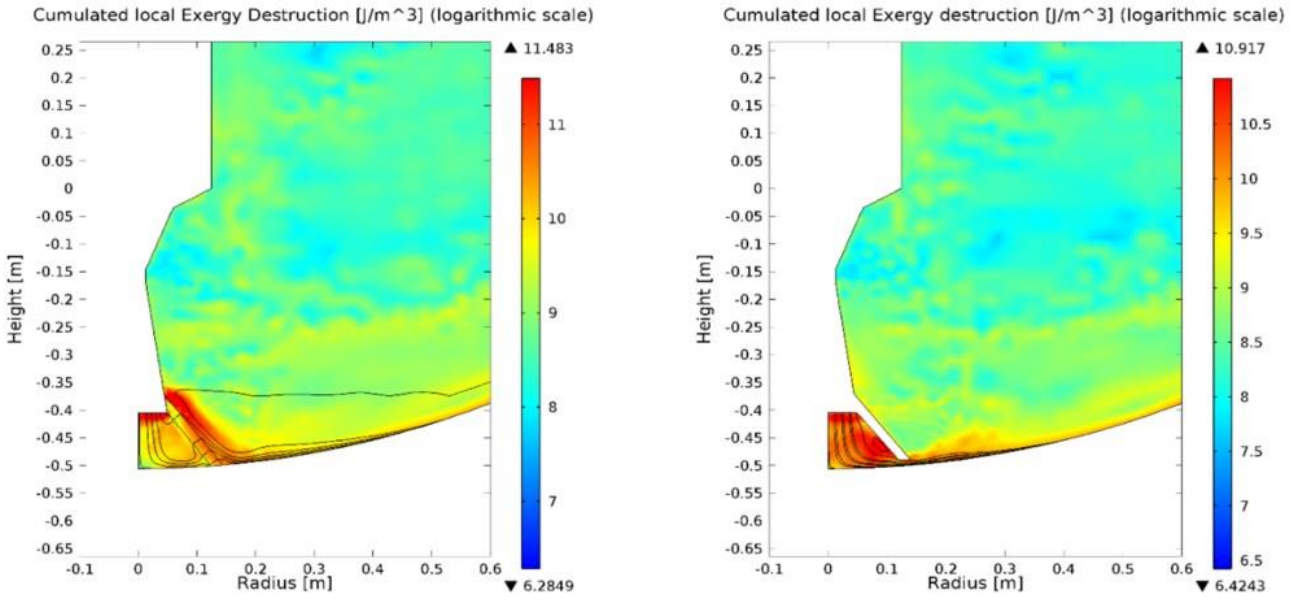

Figure 3. Cumulated exergy destroyed distribution (logarithmic scale) in the region close to the inlet with a porous baffle (left) and a solid baffle (right).

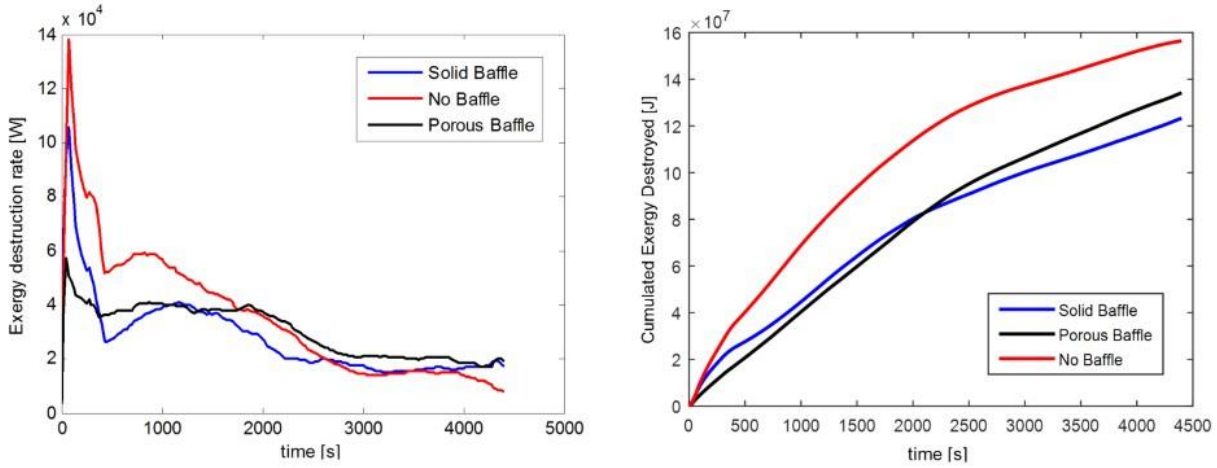

Figure 4. Left: Rate of global exergy destruction in the three cases considered. Right: Cumulated global exergy destruction in the three cases considered.

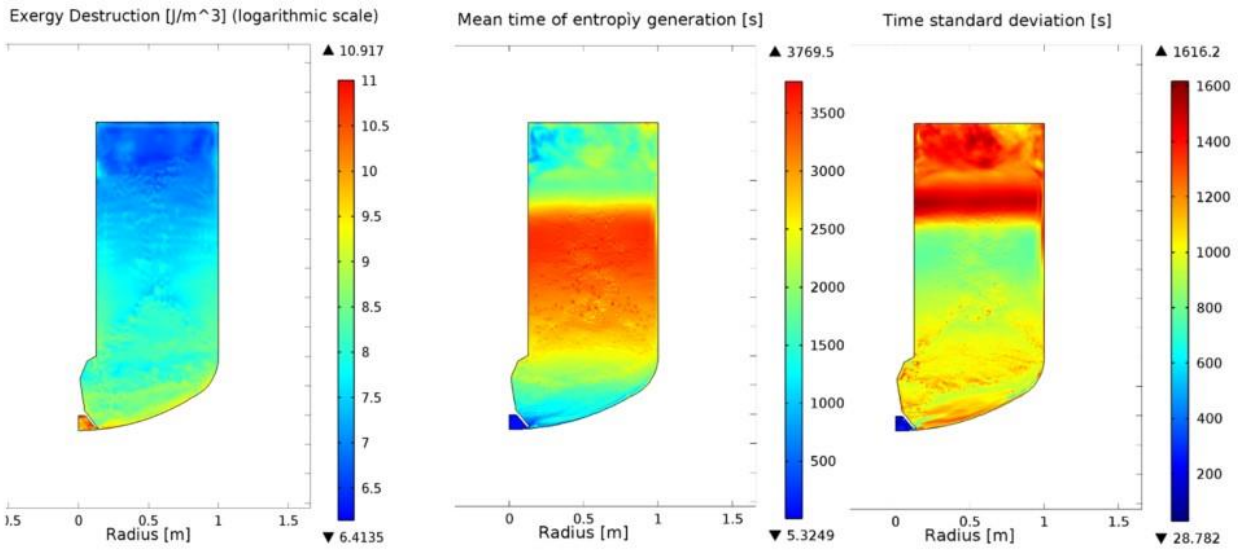

Figure 5. Analysis of the solid baffle case. Left: Cumulated entropy generation at the end of the process. Centre: Characteristic time of entropy generation. Right: Standard deviation of entropy generation

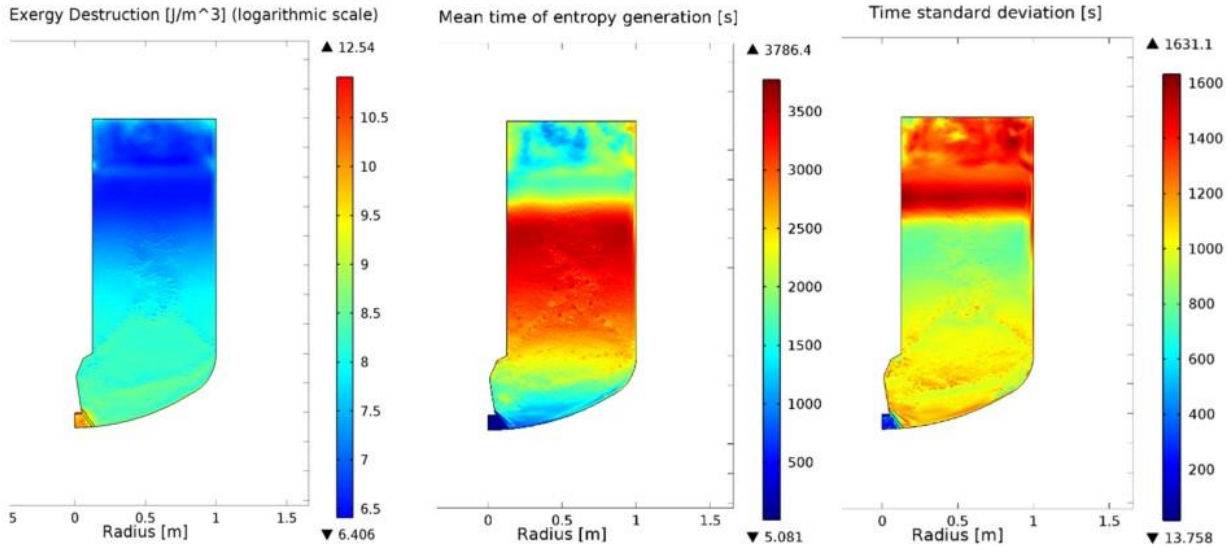

Figure 6. Analysis of the porous baffle case. Left: Cumulated entropy generation at the end of the process. Centre: Characteristic time of entropy generation. Right: Standard deviation of entropy generation

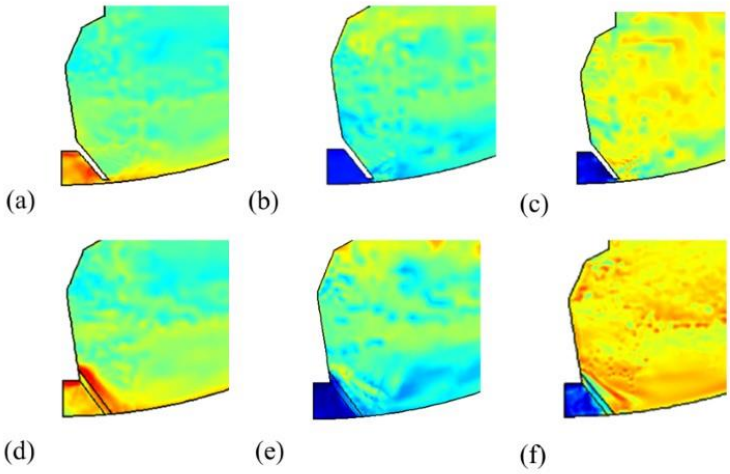

Figure 7. Local EGA of the inlet region. Left: cumulated exergy destruction with solid (a) and porous baffle (d). Center: Characteristic time of entropy generation with solid (b) and porous baffle (e). Right: Lifespan of entropy generation with solid (c) and porous baffle (f)

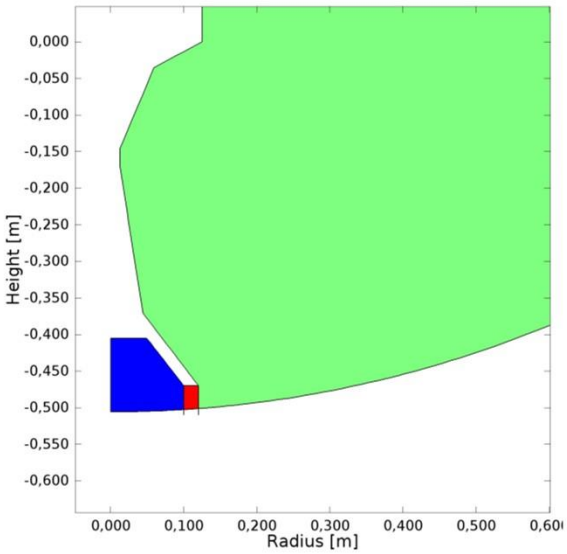

Figure 8. Geometry representation of the final design, i.e. the compounded baffle. The porous region is highlighted in red

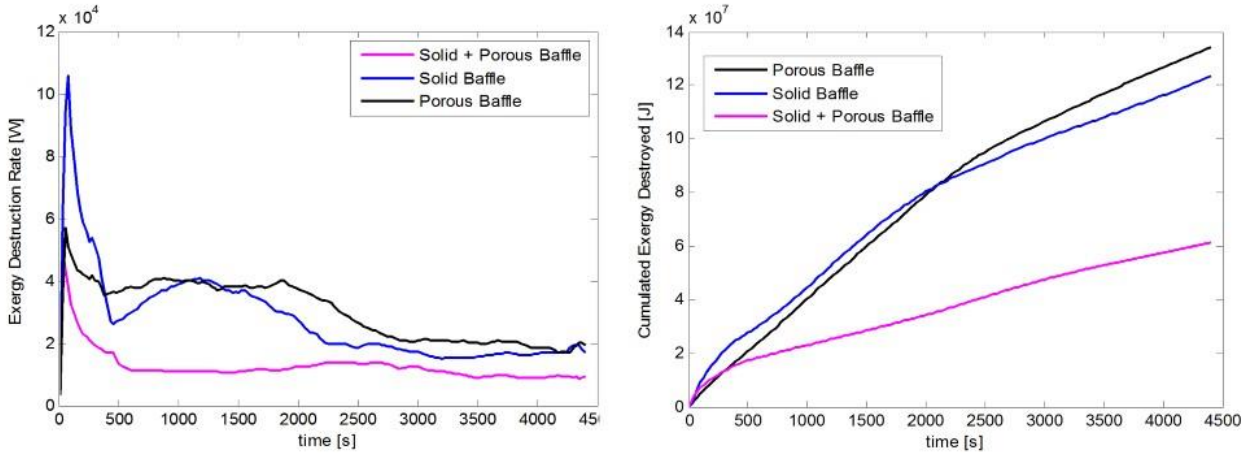

Figure 9. Performance comparison of the final design with respect to the other improvements proposed. Left: Rate of global exergy destruction Right: Cumulated global exergy destruction